Solar Light Activation of Persulfate by TiO2/Fe2O3 Layered Composite Films for Degradation of Amoxicillin: Degradation Mechanism, Matrix Effects, and Toxicity

ADVANCED SUSTAINABLE SYSTEMS
www.advsustainsys.com

# Solar Light Activation of Persulfate by $TiO_2/Fe_2O_3$ Layered Composite Films for Degradation of Amoxicillin: Degradation Mechanism, Matrix Effects, and Toxicity Assessments

*Francis M. dela Rosa, Josipa Papac, Sara Garcia-Ballesteros, Marin Kovačić, Zvonimir Katančić, Hrvoje Kušić,* and Ana Lončarić Božić*

**In this study, sandwich-type composites made of commercial $TiO_2$-P25 and $\alpha$-$Fe_2O_3$ are obtained by spin coating thin films with different layer configurations, namely: i) $TiO_2$ layer over $\alpha$-$Fe_2O_3$ ($TiO_2$@$\alpha$-$Fe_2O_3$), ii) $\alpha$-$Fe_2O_3$ layer over $TiO_2$ ($\alpha$-$Fe_2O_3$@$TiO_2$), and iii) physically mixed 50% (w/w) of $TiO_2/Fe_2O_3$. Photocatalytic activity under simulated solar irradiation of the aforementioned composites and their pure components is investigated for the degradation of amoxicillin (AMX) in the presence and absence of persulfate (PS). In both cases, $TiO_2$@$\alpha$-$Fe_2O_3$ sandwich-type achieve the highest degradation rates of AMX and a marked effect of PS addition on the AMX degradation rate is noted. The influence of pH and PS concentration on AMX degradation rate is established by means of experimental design and response surface modeling. The AMX degradation pathway is studied by means of reactive oxygen species scavenging and identification of intermediates by liquid chromatography with tandem mass spectrometry. Their evolution is directly correlated with an increased toxicity assessed by *Daphnia magna* and *Vibrio fischeri* assays. Furthermore, biodegradability changes are correlated with the mineralization profile of AMX solution. The influence of water matrix constituents ($Cl^-$, $CO_3^{2-}$, $NO_3^-$, $PO_4^{3-}$ and Suwannee river natural organic matter) on AMX degradation is established as well.**

## 1. Introduction

The occurrence of trace amounts of antibiotics in various bodies of water was directly linked to the development of antibiotic-resistant pathogens. Over the last two decades, penicillins have been widely prescribed and used across Europe.[1] In 2009, amoxicillin (AMX) alone and co-amoxiclav (combination of AMX and clavulanic acid) represented total outpatient use of 39.0 and 44.9%, respectively.[1] The high level of consumption as well as excretion rates (80–90%)[2] of unmetabolized AMX in humans accounts for an ubiquitous presence of these pharmaceutical urban wastewaters.[3–5] As such, AMX was added to the second EU "watch list" based on the proposed European Decision 2018/840/EU.[6,7] Its presence in wastewater effluents (0.05 μg $L^{-1}$)[4] is related to limited removal by common municipal wastewater treatment plants (WWTP's) based on primary (physical) and secondary (biological) treatment. Therefore, new remediation techniques must be applied to remove such recalcitrant substances.

Recently, advanced oxidation processes (AOPs) have gained much research attention due to their innate ability to provide effective oxidation of a wide variety of organic pollutants persistent to conventional WW treatment methods.[8] AOPs effectiveness rely on highly reactive and non-selective species, that can be formed either in situ or via added oxidants (hydrogen peroxide, persulfate salts, and percarbonates). Those are primarily hydroxyl radicals (HO•), although

F. M. dela Rosa, J. Papac, Dr. S. Garcia-Ballesteros, Prof. M. Kovačić, Prof. Z. Katančić, Prof. H. Kušić, Prof. A. L. Božić
Faculty of Chemical Engineering and Technology
University of Zagreb
Marulićev trg 19, Zagreb 10000, Croatia
E-mail: hkusic@fkit.hr

The ORCID identification number(s) for the author(s) of this article can be found under https://doi.org/10.1002/adsu.202100119.



**DOI: 10.1002/adsu.202100119**

F. M. dela Rosa
Catalan Institute for Water Research (ICRA)
C/Emili Grahit, 101, Girona 17003, Spain

F. M. dela Rosa
University of Girona
Girona 17071, Spain

Dr. S. Garcia-Ballesteros
Departamento de Ingeniería Textil y Papelera
Campus de Alcoy
Universitat Politècnica de València
Alcoy E-03801, Spain

Prof. H. Kušić
University North
Trg dr. Žarka Dolinara 1, Koprivnica 48000, Croatia

various other radical species might be formed depending also on the present oxidants and/or water matrix constituents: $HO_2$•, $O_2$•$^-$, Cl•, $CO_3$•$^-$, $NO_3$•, $SO_4$•$^-$, etc. Among various AOPs, semiconductor photocatalysis greatly attracts attention due to the stability of the semiconductor material and the potential to use abundant solar energy to degrade organic pollutants.[9]

The most widely investigated and employed photocatalyst in water purification is $TiO_2$, exhibiting i) high photocatalytic activity under incident photon wavelengths of $300 < \lambda < 390$ nm, and ii) satisfactory multi-functional application properties, such as chemical and thermal stability, resistance towards degradation due to hydrolysis and photocorrosion, and suitable mechanical properties.[10,11] However, $TiO_2$ suffers from the fast recombination of photogenerated charges (i.e., electron/hole pairs; $e^-/h^+$) and is only active under UV light due to its wide bandgap (3.0–3.2 eV), thus hindering its potential for solar-driven applications. These deficiencies can be improved by the following strategies: doping with metals and/or non-metals, dye sensitization, incorporation with carbon nanotubes, reduced graphene oxide, and coupling with other semiconductors with narrow bandgaps.[11–14] Coupling of $TiO_2$ with narrow bandgap semiconductors with a visible light response may promote synergistic effects between two semiconducting materials leading to more efficient charge separation and high photocatalytic activity under visible light irradiation. Iron oxide ($\alpha$-$Fe_2O_3$, also known as hematite) is a promising candidate for coupling with $TiO_2$, due to its abundance, low cost, stability in a wide-range of pH in aqueous solutions,[15] and visible light activity due to its narrow bandgap (2.0–2.2 eV). Most importantly, suitable band-edge positions of hematite promote photogenerated charge separation in $TiO_2$ via heterojunction transfer.[16,17] Despite several photocatalytic applications of $TiO_2/Fe_2O_3$ composites for the removal of contaminants of emerging concern (CECs),[17,18] all studies investigated their applications in the suspension (i.e., employing a powdered form of photocatalyst), while the application of immobilized $TiO_2/Fe_2O_3$ composites is scarcely reported. Immobilization of photocatalysts on various supports provides a potential decrease in operating costs for water treatment processes by avoiding in-treatment agglomeration and post-treatment separation issues.[10,12,19,20] Another strategy to improve $TiO_2$-based photocatalyst effectiveness is the addition of electron acceptors such as persulfate, ($S_2O_8^{2-}$, PS) which reduce $e^-/h^+$ recombination, thus leading to the increased availability of photogenerated $h^+$ for subsequent oxidation reactions and generation of additional reactive oxygen species (ROS).[21–23] However, to the best of our knowledge, solar-$TiO_2/Fe_2O_3$/PS system for AMX degradation has not yet been studied.

Herein, the aim of the study was to provide an insight on AMX removal by solar photocatalytic activation of PS using $TiO_2/Fe_2O_3$ layered films made of commercially available nanomaterials. The effect of photocatalyst layer configuration, along with the influence of initial pH and PS concentration, on AMX degradation kinetics were investigated. Besides, the mechanism of AMX degradation was investigated using common scavenging agents for formed ROS. The influence of water matrix constituents on AMX degradation was investigated as well. Finally, environmental aspects of the treatment process such as mineralization, biodegradability, and toxicity profiles were correlated with identified AMX degradation by-products.

## 2. Experimental Section

### 2.1. Chemicals

AMX ($C_{16}H_{19}N_3O_5S$, 96%, Acros Chemicals) as a targeted contaminant of emerging concern. Aeroxide P25 ($TiO_2$-P25, Evonik) and iron (III) oxide nanopowder ($\alpha$-$Fe_2O_3$, <50 nm particle size, Sigma-Aldrich) were used for the preparation of layered photoactive composites. Ethanol ($C_2H_5OH$, EtOH, 96%, Gram-mol), titanium isopropoxide ($Ti\{OCH(CH_3)_2\}_4$, TTIP, 97%, Sigma-Aldrich), perchloric acid ($HClO_4$, 70%, Kemika), tetraethyl orthosilicate ($Si(OC_2H_5)_4$, TEOS, 99%, Sigma-Aldrich), hydrochloric acid (HCl, 37%, Gram-mol), and Levasil 200/30 (colloidal $SiO_2$, Obermeier) were used for the immobilization of commercial nanoparticles onto glass substrates. Formic acid (HCOOH, FA, HPLC grade, Sigma-Aldrich) and acetonitrile ($CH_3CN$, HPLC grade, J.T. Baker) were used to prepare HPLC mobile phases. Sodium persulfate ($Na_2S_2O_8$, PS, ≥99.0%, Sigma-Aldrich) was used as an oxidant. Potassium iodide (KI, p.a., Carlo Erba) and sodium hydrogen carbonate ($NaHCO_3$ p.a., Kemika) were used for monitoring of persulfate concentration using spectrophotometric measurements. Iron (II) sulfate heptahydrate ($FeSO_4 \times 7H_2O$, ≥99.0%, Fluka), 1,10-phenanthroline monohydrate ($C_{12}H_8N_2 \times H_2O$, p.a., Kemika), sodium acetate ($NaCH_3COO$, p.a., Kemika), and acetic acid ($CH_3COOH$, ≥99.7%, Sigma-Aldrich) were used for monitoring $Fe^{2+}$, while iron (III) nonahydrate ($Fe(NO_3)_3 \times 9H_2O$, ≥98.0%, Fluka), potassium thiocyanate (KSCN, p.a., Gram-mol), and HCl, (37%, Gram-mol), for $Fe^{3+}$ concentrations by spectrophotometric techniques. Sodium hydroxide (NaOH, p.a., Kemika) and sulfuric acid ($H_2SO_4$, p.a., Kemika) were used for pH adjustments. Sodium carbonate ($Na_2CO_3$), sodium chloride (NaCl), sodium nitrate ($NaNO_3$), and di-sodium hydrogen phosphate dihydrate ($Na_2HPO_4 \times 2H_2O$) of p.a. grade obtained from Kemika, and humic acid (HA, Suwannee river, International Humic Substances Society, USA), as a natural organic matter (NOM) representative, were used to simulate the water matrix. Methanol ($CH_3OH$, MeOH, HPLC grade, J.T. Baker), tert-butanol ($(CH_3)_3COH$, *t*-BuOH, 99%, Lach-Ner), FA (98%, Fluka), and 1,4-benzoquinone ($C_6H_4O_2$, BQ, 98%, Fluka), were used for scavenging studies, that is, for the determination of main species/mechanisms involved in the degradation of AMX by studied system. In the entire study, all aqueous solutions were prepared by MilliQ-water, obtained from a Direct-Q3 UV (Merck Millipore) ultrapure water system.

### 2.2. Preparation of Layered Photocatalysts

Commercial photocatalyst nanopowders were immobilized on round glass substrates ($r$ = 37.5 mm) using a low-temperature method.[19] The procedure involved the preparation of a titania sol and silica sol. The titania-sol was prepared by $HClO_4$ catalyzed hydrolysis of TTIP in EtOH under reflux for 48 h. The silica sol was prepared by hydrolysis of TEOS in water catalyzed by HCl, conducted under constant stirring until a clear sol was obtained. Thereafter, the obtained titania sol, silica sol, Levasil200/30, and EtOH were mixed to form a binder sol. Approximately, 1.0 g of commercial photocatalyst ($TiO_2$-P25 or

$\alpha$-$Fe_2O_3$) was added to binder sol and the mixture was homogenized in an ultrasonic bath for 10 min prior to the coating. The (photocatalyst-binder sol) mixture was deposited on round glass substrates by spin coating at 1500 rpm for 30 s using a KW-4A spin coater (Chemat Technology, USA). The single-layer immobilized photocatalysts were heat-treated in an oven at 200 °C for 2h. The same procedure was repeated for preparing 2 catalyst layers, while between a coating of layers, the heating cycles (200 °C for 2 h) were applied. Configurations of the layered films were as follows: pure $TiO_2$ (double layer), pure $\alpha$-$Fe_2O_3$ (double layer), $TiO_2$ layer over $\alpha$-$Fe_2O_3$ (i.e., $TiO_2$@$\alpha$-$Fe_2O_3$), $\alpha$-$Fe_2O_3$ layer over $TiO_2$ (i.e., $\alpha$-$Fe_2O_3$@$TiO_2$), and physically mixed 50% (w/w) of $TiO_2$/$Fe_2O_3$ composite (double layer).

### 2.3. Assessment of Morphological and Optical Properties of Layered Composites

Surface morphology and film thickness of as-prepared layered composites was studied by Scanning Electron Microscopy (SEM) using Vega III (Tescan, Czech Republic). Diffuse reflectance spectra (DRS) of the prepared layered films were measured using UV-2600i UV/Vis spectrophotometer (Shimadzu), equipped with an integrating sphere. The obtained reflectance versus wavelength spectra were transformed into the Kubelka–Munk function (KM) versus photon energy ($h\nu$) in order to calculate bandgap ($E_g$) values. The recorded spectra of pure components and layered composites were transformed via KM function for the calculation of bandgap values. The bandgap ($E_g$) values of studied photocatalytic materials were calculated from the onsets of the absorption edge using formula presented by Equation (1):[24]

$$\lambda_g = \frac{1240}{E_g} \quad (1)$$

where $\lambda_g$ is the band-gap wavelength.

### 2.4. Photocatalytic Degradation of Amoxicillin (AMX) Under Solar Irradiation

Photocatalytic treatment experiments of AMX water solution (**Table 1**) were carried out in a water-jacketed (V = 0.09 L, T = 25.0 ± 0.2 °C) batch photo-reactor illuminated by a solar simulator (Oriel Arc source, Newport; 450 W Xe lamp, Osram), equipped with a collimator and airmass filter (AM 1.5G).[20] The immobilized photocatalytic material was placed at the bottom of the reactor in contact with AMX solution under constant mixing (90 rpm) by an orbital shaker DOS-20 (NeoLab, Germany). The solution was continuously mixed for 30 min in the dark in order to achieve adsorption-desorption equilibrium, denoted as (-30), and thereafter was exposed to the simulated solar illumination. The onset of illumination was denoted as (0). During the experiments, 700 µL aliquots of samples were collected at designated time intervals and filtered through a 0.45 µm Chromafil XTRA RC (Macherey-Nagel) syringe filter and were immediately quenched with 100 µL of methanol prior to HPLC analysis as described in Subsection 2.5. Preliminary

**Table 1.** The structure and characteristics of AMX and the characteristics of AMX solution prior to the treatment (measured in this study).

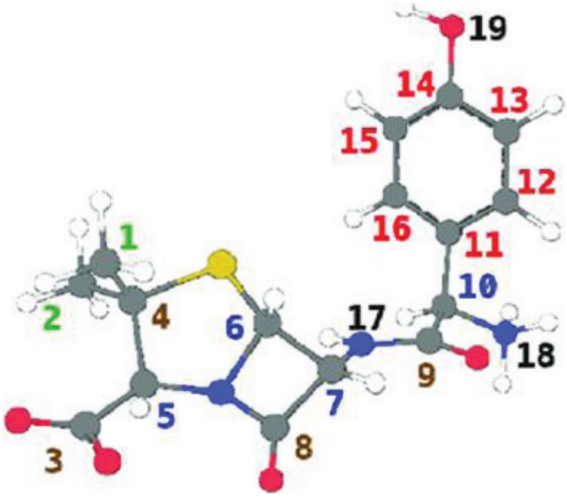


| CAS: 26787-78-0 | Aqueous solution of AMX: |
|---|---|
| Molecular formula: | Concentration: 0.05 mM |
| $C_{16}H_{19}N_3O_5S$ | $BOD_5$: 0.58 mg $O_2$ $L^{-1}$ |
| Molecular weight: | COD: 34.1 mg $O_2$ $L^{-1}$ |
| 365.4 g $mol^{-1}$ | Biodegradability ($BOD_5$/COD): 0.017 |
| Purity of standard: 96% | TOC: 9.22 mg C $L^{-1}$ |
| | Toxicity: |
| | (*Vibrio fisheri*): $EC_{50}$(15 min) = 17.79 $mgL^{-1}$, TU = 1.03 |
| | (*Daphnia magna*) $EC_{50}$(48 h) = 33.83 $mgL^{-1}$, TU = 0.54 |

experiments were carried out at AMX solution natural pH (5.5) for an illumination period of 30 min. Further study on the effect of initial pH and PS concentration was based on a full factorial experimental (FFD) plan as described in **Table 2** and Table S1, Supporting Information, where coded parameters $X_1$ and $X_2$ represent pH (ranging from 4 to 8) and concentration of PS (ranging from 50 to 500 µM), respectively. The chosen minimum and maximum concentrations of PS correspond to a AMX:PS molar ratios of 1:1 to 1:10 respectively. The obtained optimal conditions for degradation of AMX based on FFD experiments and response surface modeling (RSM) performed were utilized for the investigation of environmental parameters (i.e., mineralization, biodegradability, and toxicity), degradation by-products, scavenging studies, and the influence of water matrix parameters. Identification of reactive oxidizing species (ROS) was carried out using *t*-BuOH (5 mM), FA (5 mM), BQ (5 mM), and MeOH (5 mM) which were used as scavengers for HO•, $h^+$, $O_2$•$^-$, and both HO• and sulfate radical ($SO_4$•$^-$), respectively. Studies on the influence of water matrix parameters were carried out by spiking AMX solution with an exact concentration of the following: $\gamma(Cl^-)$ = 100 mg $L^{-1}$, $\gamma(CO_3^{2-})$ = 100 mg $L^{-1}$, $\gamma(NO_3^-)$ = 2 mg $L^{-1}$, $\gamma(PO_4^{3-})$ = 2 mg $L^{-1}$, and $\gamma$(HA) = 5 mg $L^{-1}$. In order to test the stability of $TiO_2$ / $Fe_2O_3$ layered composite films, the glass plates with immobilized catalysts showing the best performance were air-dried after the treatment and reused in four consecutive runs, employing the conditions found as optimal within the investigated range. All

**Table 2.** Experimental range and levels of process parameters/variables.

| Process parameters | Model variables/coded values | level/range | | |
|---|---|---|---|---|
| | | −1 | 0 | 1 |
| pH | $X_1$ | 4 | 6 | 8 |
| $[S_2O_8^{2-}]$ [μM] | $X_2$ | 50 | 275 | 500 |

experiments were conducted in triplicates and average values were reported; the reproducibility of experiments was ≥ 96.5%.

### 2.5. Analytical Methods

pH measurements were performed by Handylab pH/LF portable pH-meter (Schott Instruments GmbH, Mainz, Germany). AMX concentration was monitored by HPLC, Series 10, (Shimadzu, Japan) equipped with UV-DAD detector (SPD-$M10A_{VP}$, Shimadzu) using a reversed-phase (RP) C18 column (250 mm × 4.6 mm, 5 μm, Macherey-Nagel Nucleosil, Germany). Isocratic elution was carried out with a mobile phase consisting of 90% aqueous solution of 50 mM FA and 10% acetonitrile at an overall flow of 1 mL $min^{-1}$; AMX was monitored at 272 nm. AMX degradation by-products were analyzed using ultrahigh-performance chromatography, tandem with triple-quadrupole mass spectrometry on an LCMS-8045 (Shimadzu, Japan). Chromatographic separation of AMX and its degradation intermediates were achieved on an RP C18 column (150 mm × 2.1 mm Shim-pack GIST column 3 μm, Shimadzu, Japan). Gradient elution of 15 mM formic acid (A phase) and 15 mM formic acid in acetonitrile (B phase) was utilized, under the following gradient program: 0–3 min 5% B, 3–13 min 95% B, then maintained 95% B for 3 min (13–16 min) and 8 min post-run time back to the initial mobile composition (95%A/5%B). Total organic carbon (TOC) was measured using a TOC-$V_{CPN}$ analyzer (Shimadzu, Japan). A Lambda EZ 201 UV/VIS spectrophotometer (Perkin Elmer, USA) was used for spectrophotometric monitoring of PS,[25] ferrous ($Fe^{2+}$), and ferric ($Fe^{3+}$) ions concentrations.[26] Chemical oxygen demand (COD) and biochemical oxygen demand ($BOD_5$) in the samples were determined by colorimetric methods using a HACH DR2800 spectrophotometer (Hach-Lange, USA) and commercially available reagent kits, that is, LCK1414 and LCK554 (Hach-Lange) respectively. Biodegradability was expressed as $BOD_5$/COD ratio. Aquatic toxicity of treated samples was evaluated with commercial bioassays, based on *Daphnia magna* (DM) immobilization according to ISO 6341:2012 standard (Daphtoxkit F magna, Microbiotests, Belgium) and based on inhibition of the luminescence emitted by Vibrio fischeri (VF) according to ISO 11348-3:2007 measured on a BiofixLumi-10 luminometer (Macherey-Nagel, Germany).

### 2.6. Calculations

The influence of pH and PS concentration on the effectiveness of solar photocatalytic treatment was screened by means of response surface methodology (RSM). The values of process parameters are represented by independent variables: $X_1$ and $X_2$ (Table 2). Experimental space was described using $3^2$ Full Factorial Design (FFD) for solar-$TiO_2$/$Fe_2O_3$/PS system (Table S1, Supporting Information). AMX degradation rate constants after 50 min treatment period were chosen as process responses. The combined influence of studied parameters on processes performance was described by a quadratic polynomial equation representing RSM model, which was evaluated by standard statistical test, that is, analysis of variance (ANOVA) considering following statistical parameters: Fisher *F*-test value (*F*), its probability value (*p*), regression coefficients (pure; $R^2$, and adjusted; $R_{adj}^2$), *t*-test value, as well as (ii) graphical-based analysis, so-called "residual diagnostic" (RD): normal probability test, Levene's test, and constant variance test. The calculations were performed by Statistica 13.5 (Tibco); and Design-Expert 10.0 (StatEase, USA) software packages.

The calculation of PS anion HOMO and LUMO molecular orbital energy levels, with included effects of water as the solvent by the self-consistent reaction field (SCRF) method, was done using the DFT method implemented in Gaussian 16 rev. C01.[27] More details are provided in Supporting Information.

## 3. Results and Discussion

### 3.1. UV-Diffuse Reflectance Spectra of Composite Films

UV-DRS of pure components and layered composites are shown in **Figure 1**A, whereas KM transformed spectra for the calculation of bandgap values are shown in Figure 1B. As shown in **Table 3**, calculated bandgap values of commercial $TiO_2$ and $Fe_2O_3$ powders were in agreement with the literature.[28,29] For composites $TiO_2$@$\alpha$-$Fe_2O_3$ and $\alpha$-$Fe_2O_3$@$TiO_2$ the top layer contributes mostly to the total bandgap value of the composite. Moreover, the reflectance-identity of each layer can be noted in the layered, sandwich composites, that is, the distinct steep-linear regions corresponding to individual semiconductor components can be identified. The semi-transparence of the top layer in both cases enables simultaneous photo-activation of top and bottom layers. As can be seen from SEM images showing the thickness of the layers within the sandwich composites (Figure S1, Supporting Information), deposited layers are rather thin (1.06±0.20 μm), allowing the transmission of emitted light through the upper layer. The physically mixed 50% (w/w) of $TiO_2$/$\alpha$-$Fe_2O_3$ exhibited almost the same reflectance identity and bandgap value as that of pure $\alpha$-$Fe_2O_3$ (Table 3), indicating the formation of an in situ heterojunction between $TiO_2$ and $\alpha$-$Fe_2O_3$, promoted by the binding action of the immobilization.

### 3.2. Photocatalytic Degradation Experiments

Preliminary investigations of the stability of AMX towards hydrolysis, photolysis, and direct PS oxidation have shown

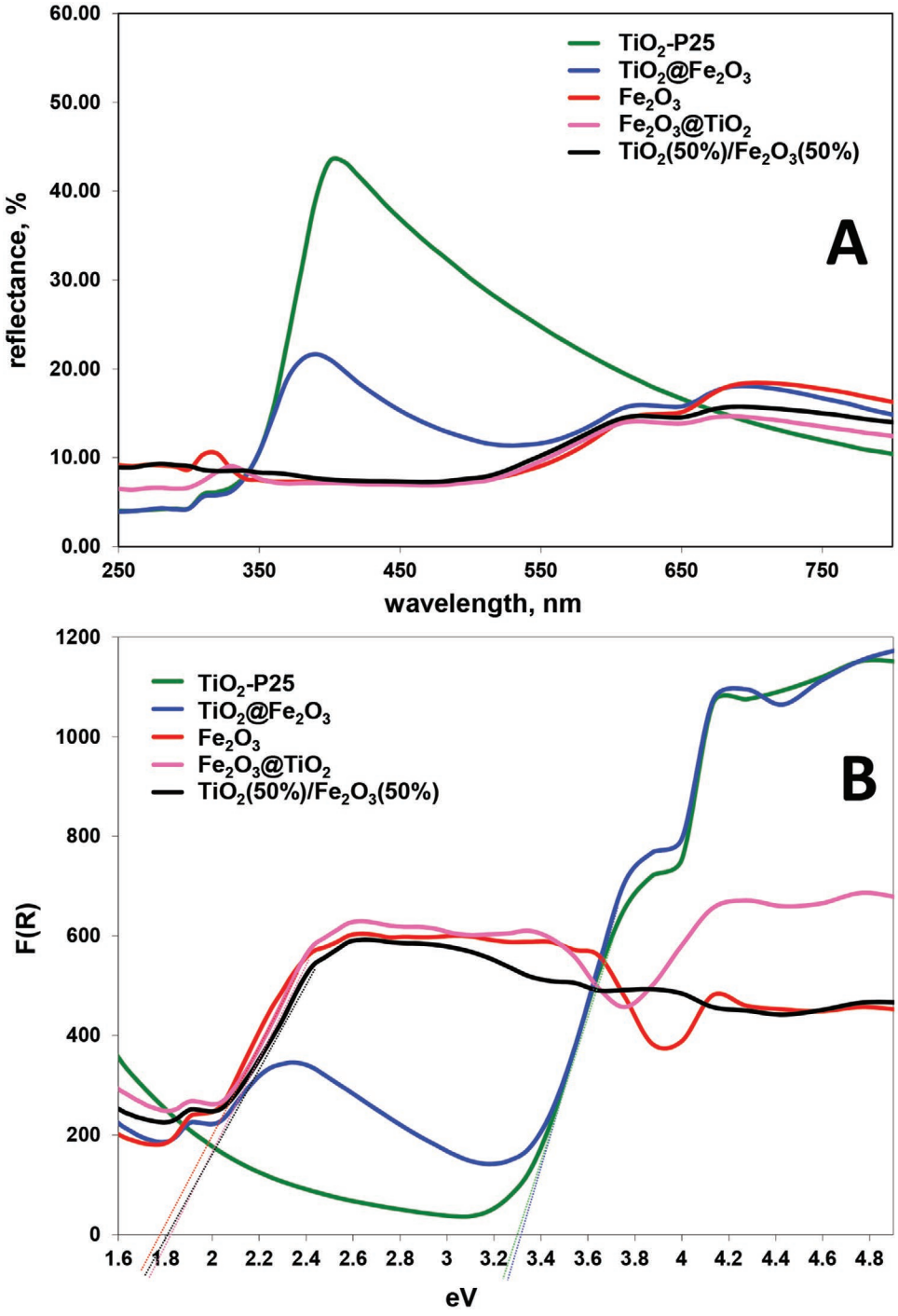


**Figure 1.** A) Diffuse reflectance spectra of coated plates; and B) corresponding plots of transformed Kubelka–Munk function versus the energy of light (eV).

**Table 3.** Photocatalyst bandgap values estimated using Kubelka–Munk function.

| Photocatalyst | $TiO_2$ (P25) | $TiO_2$@$\alpha$-$Fe_2O_3$ | $\alpha$-$Fe_2O_3$ | $\alpha$-$Fe_2O_3$@$TiO_2$ | $TiO_2$(50%)/$\alpha$-$Fe_2O_3$ (50%) |
|---|---|---|---|---|---|
| Bandgap [eV] | 3.27 | 3.30 | 1.75 | 1.80 | 1.78 |

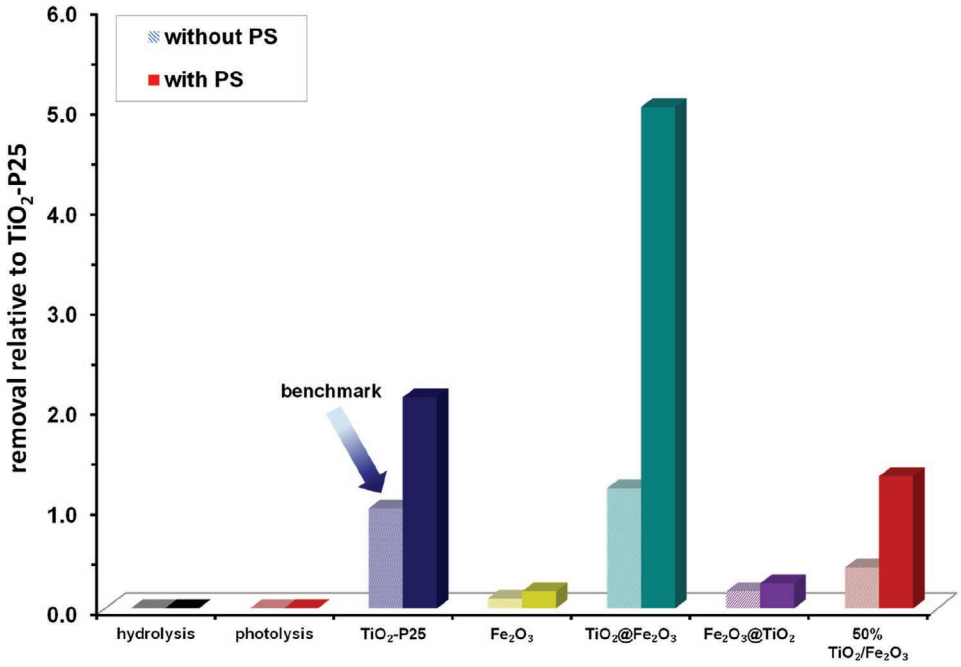


**Figure 2.** Photocatalytic degradation of AMX (50 μM) using different configurations of $TiO_2$–$Fe_2O_3$ layered composite under solar irradiation with and without PS compared relatively to benchmark $TiO_2$-P25 (experimental conditions: initial pH = natural pH, 5.5; treatment time under solar irradiation, $t$ = 30 min).

no effect on AMX concentration (**Figure 2**). The initial evaluation of photocatalytic effectiveness of the pure components and sandwich-type composites towards AMX degradation was carried out at the natural pH of AMX solution (pH 5.5), for an illumination period of 30 min after the initial dark period of 30 min allowing the achievement of the adsorption/desorption equilibrium at the photocatalyst surface. In all cases the initial adsorption extents achieved during the dark period were miniscule (<3%), hence all observed removal extents of AMX were approximated as the equivalent to the direct degradation extents. The obtained results were normalized to the degradation extent achieved by $TiO_2$-P25, considered herein as the benchmark photocatalysts (Figure 2). The highest degradation extent without the addition of PS was achieved by $TiO_2$@$\alpha$-$Fe_2O_3$, that is, 1.39-fold of TiO-P25. Such marked improvement of photocatalytic activity indicates beneficial inhibition of photogenerated $e^-/h^+$ recombination within $TiO_2$ by allowing inter-sandwich layer $e^-$ migration towards $Fe_2O_3$. Such a hypothesis is further supported by the ineffectiveness of sole $\alpha$-$Fe_2O_3$ towards AMX degradation without the presence of PS. $Fe_2O_3$ is innately unable to react directly with $H_2O$/$OH^-$, due to inadequate band edge positions of the valence and conduction bands,[18] thereby preventing the formation of HO• or other less reactive ROS, such as superoxide radical ($O_2^{\bullet-}$). According to the low adsorption extents achieved during the initial dark period, the observed degradation extents can be primarily ascribed to the reaction of ROS with AMX within the photocatalyst/solution boundary layer. Therefore, a potentially misleading synergistic effect due to the total achieved AMX degradation caused by the sum of individual contributions of $TiO_2$ and $\alpha$-$Fe_2O_3$ is effectively ruled out, strongly supporting the notion of effective charge separation by $TiO_2$@$\alpha$-$Fe_2O_3$ composite, yielding the improvement comparing to the benchmark $TiO_2$-P25 (Figure 2). On the other hand, $\alpha$-$Fe_2O_3$@$TiO_2$ sandwich composite has demonstrated inferior effectiveness in comparison to the benchmark $TiO_2$-P25, however, it is seemingly an improvement over sole $\alpha$-$Fe_2O_3$. However, the observed AMX degradation can be contributed to that achieved by $TiO_2$, which can potentially form HO• radicals, through AMX solution interface contact achieved by surface imperfections in the top $\alpha$-$Fe_2O_3$ layer, as can be observed on SEM micrographs (Figure S1, Supporting Information). Physically admixed 50% (w/w) $TiO_2$/$Fe_2O_3$ has achieved an improvement considering the effectiveness of $Fe_2O_3$@$TiO_2$, however, the AMX degradation after 30 min treatment was only 41% of that achieved by $TiO_2$-P25. Despite showing promising optical properties, in the context of filling electron states within the bandgap of $TiO_2$, $\alpha$-$Fe_2O_3$ hinders total effectiveness as it does not contribute to the formation of radicals directly, thereby effectively diluting the surface concentration of ROS formation sites. A similar effect was reported by Monfort et al.,[30] showing that $TiO_2$ (top)–$BiVO_4$ (bottom) photocatalyst layers exhibited superior activity for solar photodegradation of Rhodamine B compared to the pure $TiO_2$, $BiVO_4$, and $BiVO_4$ (top)–$TiO_2$ (bottom) layers. They concluded that such enhanced effect observed can be assigned to the formation of both $O_2^{\bullet-}$ and HO• as main oxidative species over $TiO_2$ (top) surface when irradiated with sunlight compared to $BiVO_4$ (top) which is limited to holes ($h^+$) only, having ability to form only HO•. The addition of PS has proven to be highly beneficial for $TiO_2$@$\alpha$-$Fe_2O_3$ composite, as a fivefold increase in AMX degradation was noted. The LUMO of PS is able to accept the photogenerated $e^-$ from $TiO_2$, which then leads to the generation of $SO_4^{\bullet-}$ and may lead to the formation of additional

HO•.[26] However, such a charge transfer from $\alpha$-$Fe_2O_3$ to PS is either thermodynamically or kinetically unfavorable, as can be observed by negligible improvement in photocatalytic activity of $\alpha$-$Fe_2O_3$ with the addition of PS (Figure 2). The molecular orbital configuration of PS anion obtained by DFT calculation, along with included solvation (SCRF) effects, indicates that the LUMO energy level of PS anion in the ground state is equal to –0.49 eV (Table S2, Supporting Information). Since the calculated LUMO of PS is significantly more negative than that of $\alpha$-$Fe_2O_3$,[18] such a result supports the notion that photogenerated electron transfer from pristine $\alpha$-$Fe_2O_3$ to PS is thermodynamically unfavorable. Therefore, as photocatalytic activation of PS by immobilized $\alpha$-$Fe_2O_3$ and direct degradation of AMX are not observed, it can be concluded that $\alpha$-$Fe_2O_3$ serves solely as a sink for $h^+$ and $e^-$ photogenerated within $TiO_2$ thereby enhancing its activity. Ismail et al.[31] suggested that there is a competition between the present pollutant, PS, and dissolved $O_2$ towards the reaction with photogenerated $e^-$ in the CB of $TiO_2$. Similarly, Wang et al.[32] observed that the addition of PS in UV/$TiO_2$ system showed a non-synergistic effect for 2-chlorobiphenyl degradation. Hence, in order to elucidate the effects of operating conditions, that is, pH and PS concentration, an experimental design and RSM approach was utilized to elucidate the performance of $TiO_2$@$\alpha$-$Fe_2O_3$ in combination with PS for AMX degradation kinetics. As can be seen from the kinetic profiles of AMX degradation obtained by solar-$TiO_2$/$Fe_2O_3$/PS system (experiment performed at conditions set by $3^2$ FFD, Table 2 and Table S1, Supporting Information), degradation during the period under solar irradiation obey zero-order kinetics and can be displayed with Equation (2), representing the functional dependence of AMX degradation versus treatment time, implying a surface reaction mechanism for the activation of PS.[33–35]

$$c_0 - c = -k_{obs} \times t \quad (2)$$

By applying RSM modeling, misleading information obtained from conventional "one-parameter-at-the-time" approach would be avoided.[12] FFD matrix is summarized in Table S1, Supporting Information, along with the obtained AMX degradation rate constants after 50 min of exposure to simulated solar irradiation ($k_{obs}$), which were used as system responses. It should be noted that photocatalytic experiments were run including 30 min dark period to establish adsorption equilibrium. However, the adsorbed amount of AMX during dark period was negligible in all cases (<0.9%). Such results can be assigned to point zero surface charge of $TiO_2$-P25 ($pH_{PZC}$ = 6.5–6.7)[36–38] and pKa values of AMX ($pKa_1$ = 2.4; $pKa_2$ = 7.4; $pKa_3$ = 9.6).[39] Hence, in our applied pH range (from 4 to 8) AMX exists in two speciation forms. For pH 4 and 6, AMX is present mostly in neutral form $pK_{a1}$ (2.4)< pH < $pK_{a2}$ (7.4),[39] while $TiO_2$ net surface charge is positive, thus leading to less attraction between two moieties. Furthermore, at pH 8, the net charge of $TiO_2$ and AMX are both negative implying repulsion between two moieties and leads to poor adsorption. Such a low adsorption in all cases allowed us to use zero-order $k_{obs}$ as treatment responses. Hence, the multiple regression analysis was applied on FFD matrix and $k_{obs}$(AMX) values calculated for the treatment period under simulated solar irradiation (Table S1, Supporting Information), yielding polynomial equation, that is, RSM model (3).

$$Y = 5.13 - 2.06 \times X_1 + 0.10 \times X_1^2 + 0.88 \times X_2 - 1.61 \times X_2^2 + 0.037 \times X_1 \times X_2 \quad (3)$$

The obtained model is characterized by ANOVA (Table S2, Supporting Information) and RD tools (Figure S1, Supporting Information). Basically, a model was found to be significant ($p$ = 0.0089), and accurate ($R^2$ = 0.981 and $R_{adj}^2$ = 0.949), while RD revealed that i) there are no violations in the assumptions that errors are normally distributed and independent of each other, ii) the error variances are homogeneous, and iii) residuals are independent. Accordingly, such a model can be used hereinafter as a tool to enlighten the influence of studied parameters (initial pH and PS concentration) on AMX degradation.

The ANOVA analysis also revealed that model terms corresponding to both studied process parameters are significant, that is, possess $p$ < 0.05 (Table S2, Supporting Information); thus, the changes in both initial pH and PS concentration significantly contributes to the effectiveness of solar-$TiO_2$/$Fe_2O_3$/PS system to AMX degradation. Such behavior can be clearly seen from the 3D surface and contour representation of the influence of initial pH and PS concentration on AMX degradation rate ($k_{obs}$), provided in **Figure 3**. As can be observed from Figure 3, acidic pH values are favorable for AMX degradation, thus it can be ascribed to the high concentration of $SO_4^{\bullet-}$ ($E_o$ = 2.5–3.1 V vs NHE)[40] which has higher oxidation potential than HO• ($E_o$ = 1.89–2.72 V vs NHE).[40] AMX degradation rate strongly decreases with the increase of initial pH, regardless of the PS concentration in the system. Such behavior can be also assigned to the predominant species existing in the system, which is also pH depending effect. For instance, at acidic pH (pH 4 and 6) sulfate radicals are dominant as described by

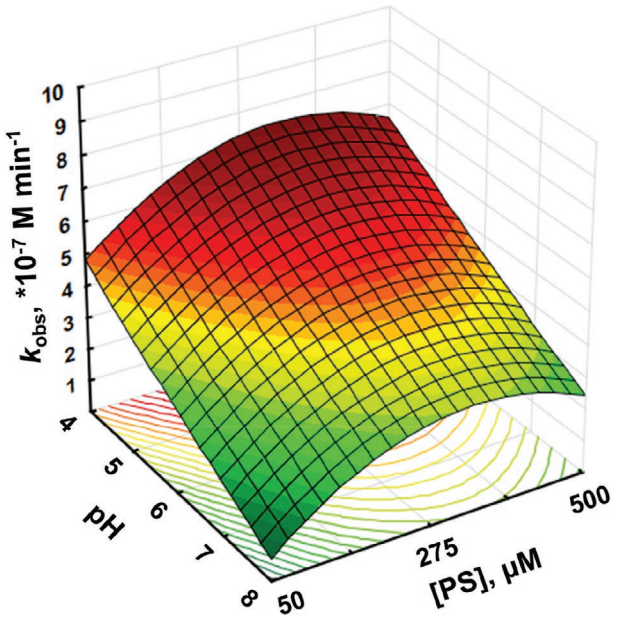


**Figure 3.** 3D surface and contour plots presenting mutual interactions of initial pH and [PS] on AMX degradation by solar-$TiO_2$/$Fe_2O_3$/PS.

Equations (4) and (5).[41,42] On the other hand, at basic pH, $SO_4^{\bullet-}$ is converted to HO• as described by Equation (6):[43]

$$S_2O_8^{2-} + H^+ \rightarrow HS_2O_8^- \quad (4)$$

$$HS_2O_8^- \rightarrow SO_4^{\bullet-} + HSO_4^{\bullet} \quad (5)$$

$$SO_4^{\bullet-} + OH^- \rightarrow OH\bullet + SO_4^{2-} \quad (6)$$

On the other hand, PS concentration effect is twofolded; by an increase of PS concentration, process effectiveness (i.e., AMX degradation) increases up to the certain point where further increase has a negative influence. The increase of PS concentration can be beneficial for the decrease of recombination rate and generation of sulfate radicals in the system. However, at too high a concentration of PS, its scavenging nature toward present radical species comes forth (Equations (7) and (8)).[26]

$$S_2O_8^{2-} + SO_4\bullet^- \rightarrow S_2O_8\bullet^- + SO_4^{2-} \quad (7)$$

$$S_2O_8^{2-} + HO\bullet \rightarrow HSO_4^- + SO_4\bullet^- + 0.5O_2 \quad (8)$$

Besides, too high concentration of radical species may promote their termination, as presented by Equations (9) and (10).[26]

$$SO_4^{\bullet-} + SO_4^{\bullet-} \rightarrow S_2O_8^{2-} \quad (9)$$

$$SO_4^{\bullet-} + OH\bullet \rightarrow HSO_4^- + \frac{1}{2}O_2 \quad (10)$$

Accordingly, as can be seen (Figure 3), the most beneficial conditions for AMX degradation are pH 4 and PS concentration of approx. 330 μM, which was accurately calculated to be 334 μM by maximizing the polynomial Equation (3), thus predicting AMX degradation at the zero-order rate of $7.4 \times 10^{-7}$ M min$^{-1}$. Such conditions were further utilized during the investigation of AMX degradation mechanism, pathway, and related changes in biodegradability and toxicity, as well as the influence of common water matrix constituents.

### 3.3. Degradation Mechanism

In order to study the degradation mechanism of AMX by solar-$TiO_2$/$Fe_2O_3$/PS system, the experiments were performed at previously established optimal conditions within the investigated range of studied process parameters and in the presence of common ROS scavengers. Hence, the quantification of the levels of oxidation by ROS was performed using the following scavengers: MeOH and *t*-BuOH to differentiate the contributions of $SO_4\bullet^-$ and HO•. Namely, MeOH reacts with both $SO_4\bullet^-$ and HO• ($k = 1.1 \times 10^7$ M$^{-1}$ s$^{-1}$ and $k = 9.7 \times 10^8$ M$^{-1}$ s$^{-1}$, respectively).[44,45] Meanwhile, *t*-BuOH reacts with HO• at a much higher rate, even three orders of magnitude ($k = (3.8–7.6) \times 10^8$ M$^{-1}$ s$^{-1}$) compared to that for $SO_4\bullet^-$ ($k = (4.0–9.1) \times 10^5$ M$^{-1}$ s$^{-1}$), thus exhibiting effective scavenging effect for HO•.[21] BQ reacts with $O_2\bullet^-$ ($k = (0.9–1.0) \times 10^9$ M$^{-1}$ s$^{-1}$) and with HO• ($k = 6.6 \times 10^9$ M$^{-1}$ s$^{-1}$),[46] while FA was used for photogenerated $h^+$ scavenging.

**Figure 4** shows AMX degradation and kinetic profiles achieved by solar/$TiO_2$/$Fe_2O_3$/PS in the presence and absence of ROS scavengers. It can be observed that the highest inhibition of AMX degradation occurred in the presence of FA. AMX degradation was reduced from 70% (no scavengers) to only 12% (with FA). This indicated that photogenerated $h^+$ plays the main role in AMX degradation, despite the fact that AMX adsorption is minor, thus direct AMX oxidation by $h^+$ can be neglected. Accordingly, such results can be assigned to the suppression of recombination of charges by the presence of PS as well as the generation of ROS at $h^+$, both contributing to the overall AMX degradation. Meanwhile, it was observed that AMX degradation was reduced from 70% (no scavengers) to 39 and 54% in presence of MeOH and *t*-BuOH, respectively. Such results indicate that $SO_4\bullet^-$ plays a more significant role than HO• in the overall AMX degradation. The presence of BQ reduced AMX degradation to 64% from 70%, suggesting that $O_2\bullet^-$ had a minor role in overall AMX degradation. Thus, the arrangement of ROS in decreasing order of its role for AMX degradation by solar/$TiO_2$-$Fe_2O_3$/PS process are the following: $h^+ > SO_4\bullet^- > HO\bullet > O_2\bullet^-$.

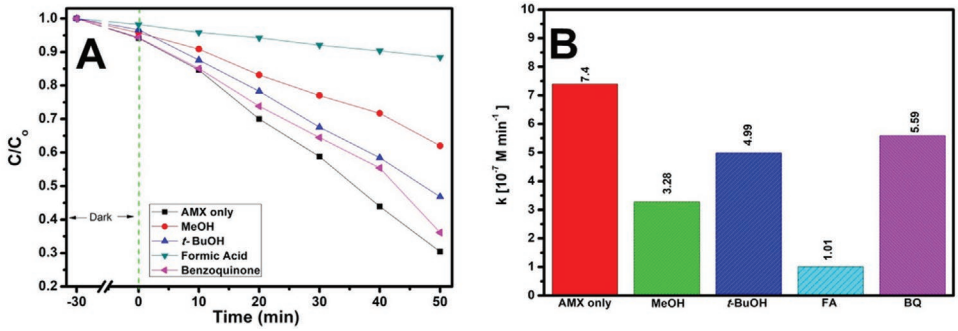


**Figure 4.** A) Photocatalytic degradation of AMX under solar irradiation in the presence of scavengers; and B) corresponding zero-order rate constants ($k_{obs}$). (experimental conditions: [AMX] = 50 μM; initial pH = 4; [PS] = 334 μM; [MeOH] = 5 mM; [*t*-BuOH] = 5 mM; [FA] = 5 mM; [BQ] = 5 mM; treatment time, $t$ = 50 min).

Similar ordering was observed by Sabri et al.[47] for another $TiO_2$-iron-PS system (vis-$TiO_2$/FeOCl/$S_2O_8^{2-}$).

### 3.4. AMX Degradation Pathway and Environmental Aspects

In order to study degradation pathway and the influence of formed by-products on the environmental aspects, that is, changes in biodegradability and toxicity, the experiments were performed for a longer period (480 min) at conditions established as optimal within the range of studied process parameters (initial pH 4 and [PS] = 334 μM). As can be seen from **Figure 5**, after 75 min >90% of AMX was degraded, while total AMX degradation was achieved within 180 min of treatment. The mineralization of organic content occurred at a much lower rate; after 75 min treatment, only 5% was mineralized, while at the treatment point where AMX was completely degraded, ≈25% of overall organic content was mineralized. It should be noted that total mineralization extent achieved after 480 min amounts to 52.2% (Figure 5A). Accordingly, the most part of the overall organic content during AMX treatment pertained to formed intermediates (e.g., after 30 min of treatment, where >50% of AMX was degraded, overall organic content is almost unchanged). Degradation of AMX is accompanied by the changes in pH (Figure 5A), which can is associated with the transformation of aromatics into aliphatic acids.[48,49] However, the decrease in pH from an initial value of 4 was only moderate due to the low strength of formed organic acids. Nevertheless, recorded pH changes (Figure 5A) display a typical pattern for degradation of organics, whereas initial decrease of pH values, associated with the formation of aliphatic acids, is followed by the slight increase as the transformation of the intermediates progresses towards final mineralization products.[50] AMX degradation and PS consumption followed similar treatment time profiles, as can be seen from Figure 5A,B. It is worth noting that PS was completely consumed up to 240 min of treatment, however, the mineralization continued to proceed with a similar rate. The consumption of PS may be associated with the increased concentration of iron species in the system, due to the fact that its presence most likely suppressed the recombination of photogenerated charges as well as hematite photocorrosion. The increased concentration of iron species may lead to the generation of HO• in the bulk through Equation (11):[26]

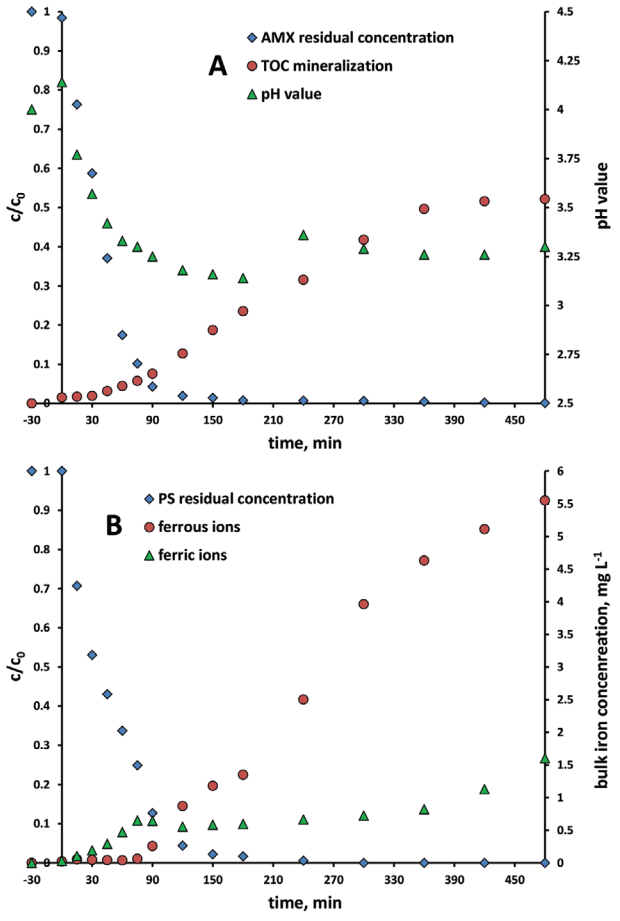


**Figure 5.** A) AMX degradation and total organic content mineralization kinetics, and changes of pH; and B) concentration of PS and iron species (ferrous/ferric ions), during AMX treatment by solar-$TiO_2$/$Fe_2O_3$/PS (experimental conditions: initial pH = 4 and [PS] = 334 μM).

$$Fe^{III}(OH)^{2+} \xrightarrow{h\nu} Fe^{2+} + HO\bullet \quad (11)$$

which additional quantity empowers the oxidative ability of the solar-$TiO_2$/$Fe_2O_3$ system over HO• mechanism. The fact that iron leaches from hematite in a form of ferric ions, and recorded profiles of ferric and ferrous ions, presented in Figure 5B, support such assumption.

The degradation pathway of AMX by solar-$TiO_2$/$Fe_2O_3$/PS was proposed in **Figure 6**; it indicates three possible degradation pathways via hydroxylation of aromatic structures and/or heteroatom(s) (N or S) involving moieties within AMX molecule. Three intermediates were detected by LC/MS/MS with molecular ion peak of ($m/z$ = 382) and base peak ($m/z$ = 365). All of the detected intermediates are ascribed to monohydroxylation of AMX.[51,52] Accordingly, DP1 was formed via attack of $SO_4^{\bullet-}$ and/or HO• to the sulfur atom of thioether moiety by electron transfer mechanism and was confirmed by molecular orbital calculations.[51] Thereafter, DP1 can proceed with further hydroxylation in the aromatic ring moiety yielding intermediate with $m/z$ = 398.[51] Meanwhile, DP2 was formed via attack of HO• to the aromatic ring of AMX. Subsequently, DP2 would undergo further hydroxylation and deamination to yield intermediate with $m/z$ = 383, and further degradation leads to smaller by-products such as $m/z$ = 176. DP3 was formed by hydroxylation of secondary amine moiety of AMX, and was further hydroxylated to form $m/z$ = 412 then subsequently degraded to form $m/z$ = 176. However, ion chromatography results revealed that there are no free N-containing ions (i.e., $NO_3^-$, $NO_2^-$, $NH_4^+$) during the entire treatment time of 480 min, suggesting that degradation products contain N-functionality. Accordingly, it seems that DP2 underwent hydroxylation step, but not an elimination of amino moiety. As compared to the literature, solar photo-Fenton and UV/PS treatment of AMX degradation proceeds via hydroxylation, hydrolysis, and decarboxylation. However, it must be noted that three monohydroxylated by-products were not detected simultaneously by the previous studies. For instance, Trovo et al.,[52] only detected DP2 and DP3, while Zhang et al.[51] only detected DP1 and DP2.

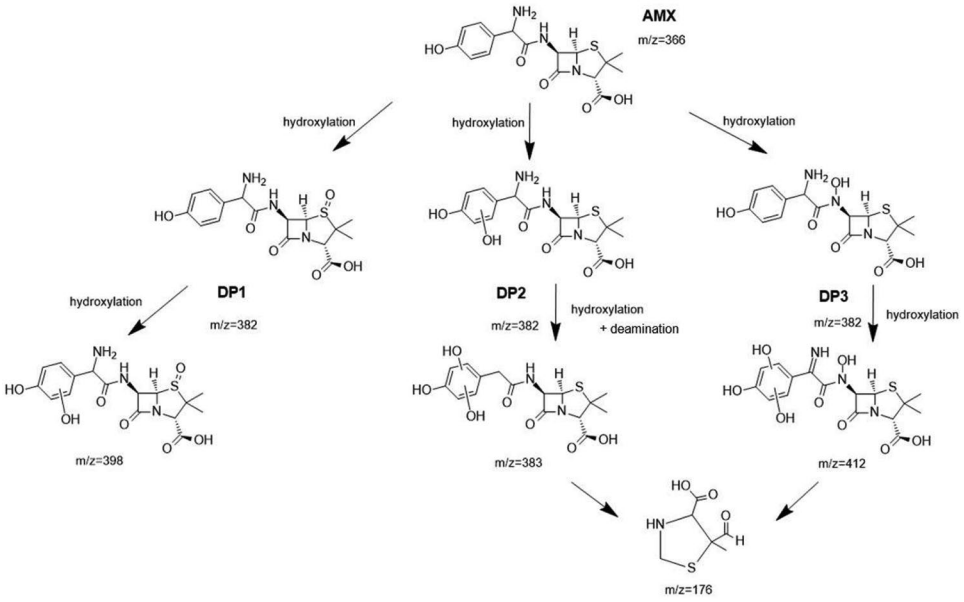


**Figure 6.** Proposed degradation pathway of AMX by solar-$TiO_2/Fe_2O_3$/PS system based on identified AMX intermediates and literature data (experimental conditions: initial pH = 4 and [PS] = 334 μM).

The evolution and degradation profiles of DP1, DP2, and DP3 are presented in **Figure 7**A and were correlated with the changes in biodegradability (Figure 7B) and toxicity (Figure 7C). As can be seen, all three identified AMX by-products followed a similar evolution/degradation pattern. Hence, their concentrations increased continuously up to 45$^{th}$ (for DP2 and DP3) and 60$^{th}$ (DP1) minute or treatment, while after those periods, their degradation rates prevailed over evolution rates, thus their concentration started to decrease during further treatment period, and eventually completely disappeared from the system after 480 min treatment (Figure 7A). Despite that, TOC value amounted after 480 min treatment to 47.8% of the initial value (Figure 5A, indicating that other unidentified AMX organic by-products were still present to a large extent. As can be seen from the proposed pathway, identified DP1, DP2 and DP3 are consequences of hydroxylation of AMX molecule (either at benzene moiety or present heteroatoms, Figure 6), while their further degradation undergoes a similar pattern, that is, via hydroxylation at benzene moiety. Accordingly, after the cleavage of C10-C11 bond (Table 1), such (poly-)hydroxylated benzene ring would then undergo degradation as phenolic-like compounds over ring-open products and would be eventually mineralized.[53] This is supported by the fact that no free N-containing ions were detected with the progress of mineralization.

As can be seen from Figure 7B, the initial AMX solution can be characterized as non-biodegradable; $BOD_5/COD = 0.017$. As it is known from the literature,[54] wastewater with $BOD_5/COD < 0.3$ are characterized as non-biodegradable, while those with $0.3 < BOD_5/COD < 0.4$ are partially biodegradable; and those with $BOD_5/COD > 0.4$ can be characterized as biodegradable. Treatment of AMX solution by solar-$TiO_2/Fe_2O_3$/PS resulted in an increase in BOD5/COD ratio. Comparing $BOD_5$/COD and mineralization profiles presented in Figure 7B and Figure 5A respectively, one may conclude that improved biodegradability is a consequence of mineralization, that is, decreases in organic content. However, that is not quite correct. Although TOC, COD, and $BOD_5$ are used as the main sum parameters to quantify the organic load, they possess different biases. Namely, TOC and COD encompass the entire organic content regardless of their structural characteristics as they measure the amount of carbon bound to organic compound and the amount of organic compound which is chemically oxidized to $CO_2$. On the other hand, susceptibility of organics to biochemical transformation encompassed in BOD is influenced by its' chemical structures. Hence, COD and TOC can only decrease during applied photocatalytic treatment, while $BOD_5$ values can either decrease or increase depending on the nature (i.e., structure) of the degradation byproducts formed. The decrease can be associated with either the formation of less biodegradable compounds or the decrease in overall organic content, while the increase in $BOD_5$ value can be only due to the formation of compounds, degradation intermediates, which are more biodegradable than the parent compound.[54] Although these profiles are similar, biodegradability increase is not the only consequence of decreased organic content. Namely, the partially biodegradable values were reached at treatment period (180 min) aligned with the complete AMX degradation and disappearance of the majority of DP1, DP2, and DP3 from the system (they were present <10% of their maximum concentration detected). Considering the proposed pathway and assumption that majority of mineralization underwent over (poly-)hydroxylated benzene moiety, which are known to be non-biodegradable,[53] the improvement of biodegradability can be associated with the degradation of such hydroxylated structures.

More clear correlation between formed DP1, DP2, and DP3 can be observed from toxicity changes, presented in Figure 7C. It should be noted that according to the toxicity categories established by the guidelines,[55] the initial AMX solution can be classified as "harmful to aquatic microorganisms"; $EC_{50}$(VB) = 17.79 mg $L^{-1}$ and $EC_{50}$(DM) = 33.83 mg $L^{-1}$. Such results are

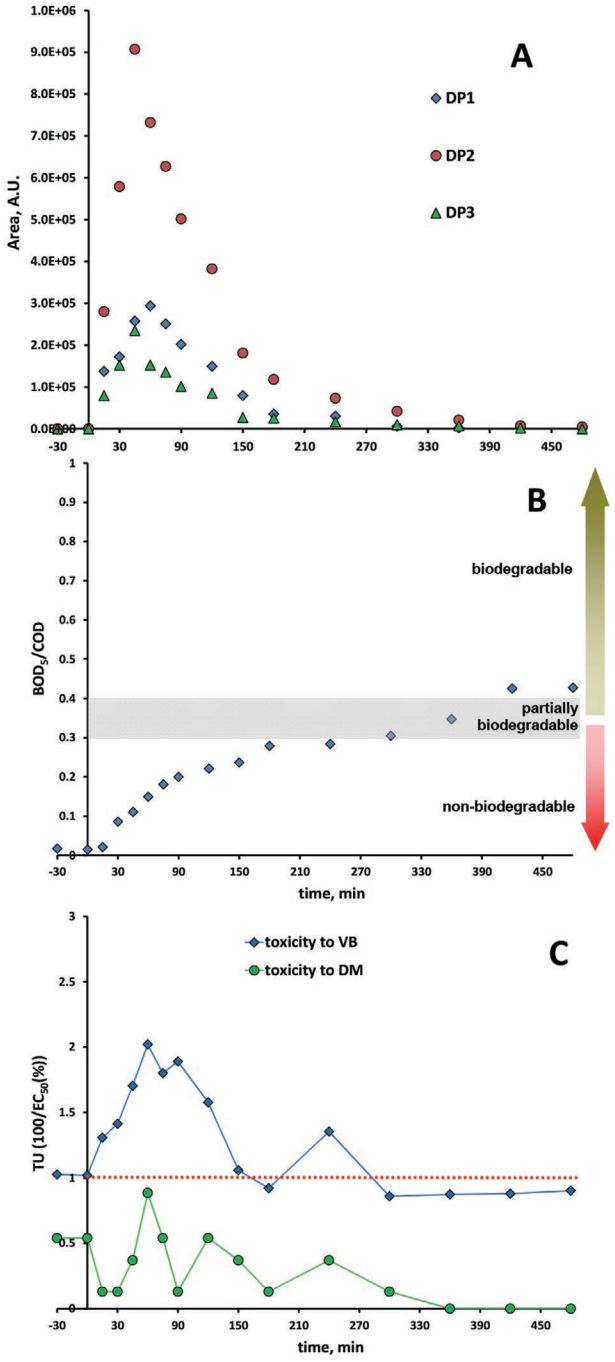


**Figure 7.** A) Evolution and degradation of identified AMX by-products; B) changes in biodegradability; and C) toxicity toward VB and DM, during AMX treatment by solar-$TiO_2$/$Fe_2O_3$/PS (experimental conditions: initial pH = 4 and [PS] = 334 μM).

generally in accordance with the literature data, which are, rather scarce; only several sources were found referring to AMX toxicity toward VB and/or DM.[52] However, these studies did not present toxicity over common parameters such as $EC_{50}$ or TU (presentation was done over single inhibition numbers), thus it is hard to compare the results from this study and available literature. The toxicity changes recorded toward both bioassays follow more or less the same trend; during the treatment period where AMX and its initial by-products DP1, DP2, and DP3 prevail in the reaction mixture (i.e., up to 180$^{th}$ minute of treatment), toxicity underwent sinusoidal increases and decreases, reaching the maximums aligned with the maximal recorded concentrations of identified by-products (i.e., at 45$^{th}$ and 60$^{th}$ min). After that period toxicity value mostly decreased, the exception is a slight increase recorded in 240$^{th}$ minute of treatment by both bioassays, which can be associated with the appearance of characteristic by-products toxic for both VB and DM. However, after that treatment period toxicity decreased <1 (in TU) and to 0 in the cases of VB and DM bioassays, respectively (Figure 7C). Obtained results indicate the strong correlation between the evolution and degradation of hydroxylated aromatic structures and the observed changes in toxicity profiles.

### 3.5. Influence of Water Matrix

In order to get an insight into the efficiency of solar-$TiO_2$/$Fe_2O_3$/PS system for the degradation of AMX in the presence of common water matrix constituents such as: carbonates, chlorides, phosphates, nitrates, and NOM in a form of HA, experiments were performed to investigate their individual and mutually combined effects. As shown in **Figure 8**A, AMX degradation was inhibited in all cases. The obtained results can be plausibly explained with the fact that added substances may react with the formed $SO_4^{\bullet-}$ and HO•, forming specific radicals which seem to be less reactive toward AMX than $SO_4^{\bullet-}$ and HO•, thus, consequently inhibiting AMX degradation through such competitive reactions. The inhibitory effect strongly depends on the reaction rates and concentrations of added substances with $SO_4^{\bullet-}$ and HO•. According to the literature,[56,57] AMX reaction rate constants with $SO_4^{\bullet-}$ and HO• are $k_{SO_4^{\bullet-}} = 2.79 \times 10^9$ $M^{-1}$ $s^{-1}$ and $k_{HO\bullet} = 6.64 \pm 1.40 \times 10^9$ $M^{-1}$ $s^{-1}$. The highest inhibitory effect toward AMX degradation was observed in the case of carbonates; $k_{obs}$ decreased by 86.0% compared to the case-referent case without water matrix constituents presence ($1.04 \times 10^{-7}$ M $min^{-1}$ << $7.40 \times 10^{-7}$ M $min^{-1}$) (Figure 8B). Taking into account that both $CO_3^{2-}$ and $HCO_3^-$ reacts rather rapidly with $SO_4^{\bullet-}$ ($k_{SO_4^{\bullet-}/HCO_3^-} = 1.6 \times 10^6$ $M^{-1}s^{-1}$ and $k_{SO_4^{\bullet-}/CO_3^{2-}} = 6.1 \times 10^6$ $M^{-1}$ $s^{-1}$)[58] and HO• ($k_{HO\bullet/HCO_3^-} = 8.5 \times 10^6$ $M^{-1}$ $s^{-1}$ and $k_{HO\bullet/CO_3^{2-}} = 3.9 \times 10^8$ $M^{-1}$ $s^{-1}$),[46] as well as the fact that carbonates concentration was 33.3 times higher than that of AMX, the inhibitory effect was not surprising. Similar is valid for chlorides as well, where $k_{obs}$ has been also diminished significantly (for 61.4%) (Figure 8B). Besides reactions with formed radical species ($k_{HO\bullet/Cl^-} = 4.3 \times 10^9$ $M^{-1}$ $s^{-1}$ and $k_{SO_4^{\bullet-}/Cl^-} = 3.1 \times 10^8$ $M^{-1}$ $s^{-1}$),[46,59] chlorides adsorption on the surface of $TiO_2$ layer may hinder the adsorption and consequently reactive sites for PS activation.[60] Namely, in solar-$TiO_2$/$Fe_2O_3$/PS process, persulfate activation occurs at the surface of the photocatalyst, thus the adsorption step is essential for the overall AMX degradation. The observed inhibitory effects in the case of nitrates and phosphates can be assigned to combined adsorption and competitive reactions, as in the case of chlorides.[60] However, as can be seen from Figure 8B, inhibitory effects were much lower than in the case of chlorides; $k_{obs}$ diminished 14.5% (with nitrates)

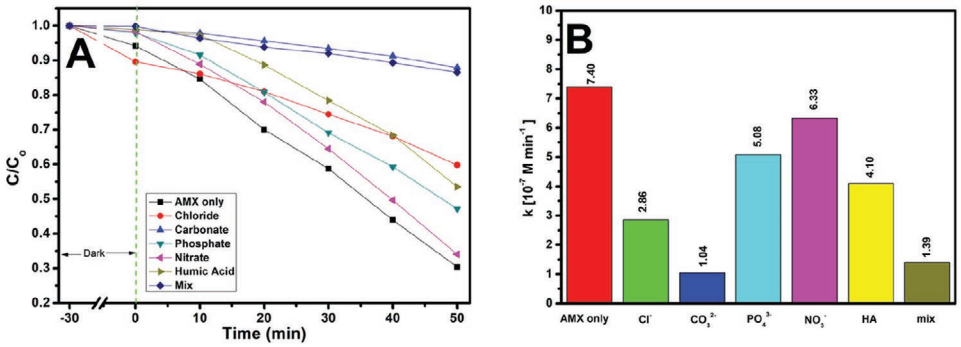


**Figure 8.** A) Photocatalytic degradation of AMX under solar irradiation in the presence of common water matrix constituents; and B) corresponding zero-order rate constants ($k_{obs}$). (experimental conditions: [AMX] = 50μM; pH = 4; [PS] = 334 μM; [$Cl^-$] = 100 mg $L^{-1}$, [$CO_3^{2-}$] = 100 mg $L^{-1}$, [$NO_3^-$] = 2 mg $L^{-1}$, [$PO_4^{3-}$] = 2 mg $L^{-1}$, and [HA] = 5 mg $L^{-1}$, treatment time, t = 50 min).

and 31.4% (with phosphates). The plausible explanation can be found in the concentrations of added nitrates and phosphates that were 80 and 130 times lower, respectively, comparing to chlorides. Their concentrations definitely affected the competitive reactions with AMX as well; nitrates and phosphates were present in 1.5 and 2.4 times lower concentrations, respectively, than AMX. The presence of NOM, represented by HA, inhibited AMX degradation rather significantly; $k_{obs}$ diminished for 44.6% ($4.1 \times 10^{-7}$ M $min^{-1} < 7.4 \times 10^{-7}$ M $min^{-1}$ (Figure 8B). It should be noted that HA, besides reacting with present radical species in the system, is susceptible to photodegradation under solar irradiation, thus introducing additional radical species that are capable to react with targeted organics. Accordingly, HA's may also provide synergistic or inhibitory effects on the removal rate of targeted compounds by photo-AOPs.[61–63] As can be concluded from the obtained results in our study, the inner filter effect of HA, which promotes the reduction of incident irradiation flux activation of photocatalytic material occurred, thus lowering AMX degradation rate. Moreover, HA is rich in electrons and could also scavenge HO• and $SO_4^{\bullet-}$ rapidly,[64,65] thus contributing to the observed inhibitory effect (Figure 8B). In addition, HA promotes the increase in a negative charge in the surface of $TiO_2$,[66] thus leading to the inhibition of PS activation, consequently lowering the overall AMX degradation rate (Figure 8B). Hence, it seems that in our case multiple negative effects of HA presence prevailed over the above-stated synergistic effect related to the formation of additional NOM-based radical species. Finally, we have also studied combined effects of all substances investigated separately, and found out that inhibitory effect is quite significant ($k_{obs}$ diminished for 81.2%, (Figure 8B), most likely as a consequence of above-explained separate effects.

### 3.6. Stability Test

In order to confirm the stability of immobilized photocatalyst, $TiO_2$@$Fe_2O_3$ composites were utilized for four consecutive degradation experiments employing optimal conditions within the studied range of parameters obtained in Subsection 3.2. As shown in **Figure 9**, AMX removal of >96% was achieved in each cycle. Gravimetric analysis revealed negligible weight loss (<0.008%), confirming excellent stability and potential to be reused. In addition, no significant changes in appearance between fresh and reused $TiO_2$@$Fe_2O_3$ immobilized composites were observed (Figure S4, Supporting Information).

## 4. Conclusions

The sandwich-type composites made of commercial $TiO_2$-P25 and $\alpha$-$Fe_2O_3$ with different layer configurations were successfully prepared by spin coating, and thereafter tested for photocatalytic activity in the presence and absence of PS under simulated solar irradiation using pharmaceutical AMX as targeted CECs.

SEM analysis showed that prepared layers within sandwich-type composites are rather thin (1.06±0.20 μm), while DRS analysis revealed the semi-transparence of the top layer enabling simultaneous photo-activation of both top and bottom layers. Such property is shown to be beneficial particularly for the activity of $TiO_2$@$Fe_2O_3$ composite, particularly in the presence of PS. Namely, $TiO_2$@$Fe_2O_3$ showed superior activity under simulated solar irradiation and PS presence among all studied composite combinations and their pure components. Such

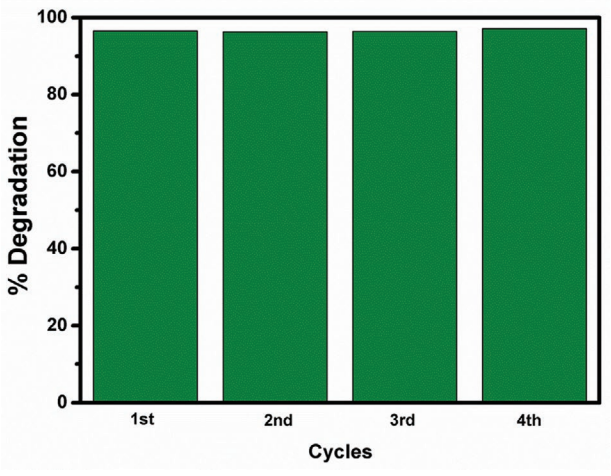


**Figure 9.** AMX removal by solar-$TiO_2$/$Fe_2O_3$/PS during four consecutive treatment cycles. (experimental conditions: initial pH = 4, [PS] = 334 μM and irradiation time = 120 min).

marked improvement of photocatalytic activity was due to the successful suppression of the recombination of photogenerated charges ($e^-/h^+$) within $TiO_2$ by allowing inter-sandwich layer migration of photogenerated $e^-$ towards $\alpha$-$Fe_2O_3$. Additionally, as revealed by DFT calculations, LUMO of PS is able to accept photogenerated $e^-$ from $TiO_2$, which then led to the generation of $SO_4^{\bullet -}$, yielding the improved AMX degradation. RSM modeling exhibited that acidic conditions are favorable for AMX degradation by solar-$TiO_2$/$Fe_2O_3$/PS process. The experiments using common ROS scavengers showed that AMX degradation was mainly driven over $SO_4^{\bullet -}$ and HO•, clearly emphasizing the important role of photogenerated $h^+$ as a result of effective suppression of charge recombination, yielding enhanced ROS generation at both $h^+$ and $e^-$. Biodegradability of AMX solution was significantly improved, while the changes observed during the treatment can be correlated mostly with mineralization kinetics, that is, decrease in overall organic content by progressed mineralization of benzene moiety of AMX molecule via hydroxylation pathway similar to that of phenolic compounds. Toxicity changes of AMX solution during solar-$TiO_2$/$Fe_2O_3$/PS treatment are correlated with (poly-)hydroxylated by-products evolution/degradation; their disappearance from the system yielded a significant toxicity decrease of treated solution.

## Supporting Information

Supporting Information is available from the Wiley Online Library or from the author.

## Acknowledgements

This paper is part of a project that has received funding from the European Union's Horizon 2020 – Research and Innovation Framework Programme under the H2020 Marie Skłodowska-Curie Actions grant agreement No. 812880. The paper reflects only the authors' view and the Agency is not responsible for any use that may be made of the information it contains.

## Conflict of Interest

The authors declare no conflict of interest.

## Data Availability Statement

Research data are not shared.

## Keywords

amoxicillin, persulfate, sandwich-type composite photocatalysts, solar irradiation, toxicity

Received: April 17, 2021
Revised: June 11, 2021
Published online: July 16, 2021

[1] A. Versporten, S. Coenen, N. Adriaenssens, A. Muller, G. Minalu, C. Faes, V. Vankerckhoven, M. Aerts, N. Hens, G. Molenberghs, H. Goossens, S. Metz, G. Fluch, S. Vaerenberg, M. M. Goossens, *J. Antimicrob. Chemother.* **2011**, *66*, 13.
[2] R. Hirsch, T. Ternes, K. Haberer, K. L. Kratz, *Sci. Total Environ.* **1999**, *225*, 109.
[3] R. Andreozzi, V. Caprio, C. Ciniglia, M. De Champdoré, R. Lo Giudice, R. Marotta, E. Zuccato, *Environ. Sci. Technol.* **2004**, *38*, 6832.
[4] A. J. Watkinson, E. J. Murby, D. W. Kolpin, S. D. Costanzo, *Sci. Total Environ.* **2009**, *407*, 2711.
[5] H. W. Leung, T. B. Minh, M. B. Murphy, J. C. W. Lam, M. K. So, M. Martin, P. K. S. Lam, B. J. Richardson, *Environ. Int.* **2012**, *42*, 1.
[6] EC, Off., *J. Eur. Union* **2018**, *L 141*, 9.
[7] R. Loos, D. Marinov, I. Sanseverino, D. Napierska, T. Lettieri, *Review of the 1st Watch List under the Water Framework Directive and Recommendations for the 2nd Watch List*, Publications Office Of The European Union, Luxembourg, **2018**.
[8] S. Parsons, *Advanced Oxidation Processes for Water and Wastewater Treatment*, IWA Publishing, London, UK **2005**.
[9] M. Kovacic, H. Kusic, A. L. Bozic, D. D. Dionysiou, in: *Encyclopedia of Water: Science, Technology, and Society. Part IV Water Technology: Water Treatment and Supply*, Wiley, USA **2020**, pp. 1925–1940.
[10] J. Schneider, M. Matsuoka, M. Takeuchi, J. Zhang, Y. Horiuchi, M. Anpo, D. W. Bahnemann, *Chem. Rev.* **2014**, *114*, 9919.
[11] P. Pichat, *Photocatalysis and Water Purification:From Fundamentals to Recent Applications*, Wiley, Germany **2013**.
[12] M. N. Chong, B. Jin, C. W. K. Chow, C. Saint, *Water Res.* **2010**, *44*, 2997.
[13] M. Pelaez, N. T. Nolan, S. C. Pillai, M. K. Seery, P. Falaras, A. G. Kontos, P. S. M. Dunlop, J. W. J. Hamilton, J. A. Byrne, K. O'shea, M. H. Entezari, D. D. Dionysiou, *Appl. Catal., B* **2012**, *125*, 331.
[14] R. Fagan, D. E. McCormack, D. D. Dionysiou, S. C. Pillai, *Mater. Sci. Semicond. Process.* **2016**, *42*, 2.
[15] C. A. Lanzl, J. Baltrusaitis, D. M. Cwiertny, *Langmuir* **2012**, *28*, 15797.
[16] S. J. A. Moniz, S. A. Shevlin, X. An, Z. X. Guo, J. Tang, *Chem. - Eur. J.* **2014**, *20*, 15571.
[17] O. F. S. Khasawneh, P. Palaniandy, *Environ. Technol. Innovation* **2021**, *21*, 101230.
[18] K. Perović, F. M. dela Rosa, M. Kovačić, H. Kušić, U. L. Štangar, F. Fresno, D. D. Dionysiou, A. L. Bozic, *Materials* **2020**, *13*, 1338.
[19] M. Kete, E. Pavlica, F. Fresno, G. Bratina, U. L. Štangar, *Environ. Sci. Pollut. Res.* **2014**, *21*, 11238.
[20] M. Kovacic, N. Kopcic, H. Kusic, A. L. Bozic, *J. Photochem. Photobiol., A* **2018**, *361*, 48.
[21] J. M. Monteagudo, A. Durán, I. S. Martín, B. Vellón, *Sep. Purif. Technol.* **2020**, *238*, 116456.
[22] A. Mills, M. A. Valenzuela, *J. Photochem. Photobiol., A* **2004**, *165*, 25.
[23] S. Bekkouche, S. Merouani, O. Hamdaoui, M. Bouhelassa, *J. Photochem. Photobiol., A* **2017**, *345*, 80.
[24] D. Andrews, T. Nann, R. Lipson, *Comprehensive Nanoscience and Nanotechnology Title*, Elsevier B.V, The Netherlands **2019**.
[25] C. Liang, C. F. Huang, N. Mohanty, R. M. Kurakalva, *Chemosphere* **2008**, *73*, 1540.
[26] H. Kusic, I. Peternel, S. Ukic, N. Koprivanac, T. Bolanca, S. Papic, A. L. Bozic, *Chem. Eng. J.* **2011**, *172*, 109.
[27] M. J. Frisch, G. W. Trucks, H. B. Schlegel, G. E. Scuseria, M. A. Robb, J. R. Cheeseman, G. Scalmani, V. Barone, G. A. Petersson, H. Nakatsuji, X. Li, M. Caricato, A. V. Marenich, J. Bloino, B. G. Janesko, R. Gomperts, B. Mennucci, H. P. Hratchian, J. V. Ortiz, A. F. Izmaylov, J. L. Sonnenberg, D. Williams-Young, F. Ding, F. Lipparini, F. Egidi, J. Goings, B. Peng, A. Petrone, T. Henderson, D. Ranasinghe, V. G. Zakrzewski, J. Gao, N. Rega, G. Zheng, W. Liang, M. Hada, M. Ehara, K. Toyota, R. Fukuda, J. Hasegawa, M. Ishida, T. Nakajima, Y. Honda, O. Kitao, H. Nakai, T. Vreven, K. Throssell, J. A. Montgomery Jr., J. E. Peralta, F. Ogliaro, M. J. Bearpark, J. J. Heyd, E. N. Brothers, K. N. Kudin, V. N. Staroverov, T. A. Keith, R. Kobayashi, J. Normand, K. Raghavachari, A. P. Rendell, J. C. Burant, S. S. Iyengar, J. Tomasi, M. Cossi, J. M. Millam, M. Klene, C. Adamo, R. Cammi,

J. W. Ochterski, R. L. Martin, K. Morokuma, O. Farkas, J. B. Foresman, D. J. Fox, *Gaussian 16, Revision C.01*, Gaussian, Inc., Wallingford CT **2019**.
[28] R. G. J. Strens, B. J. Wood, *Mineral. Mag.* **1979**, *43*, 347.
[29] J. Torrent, V. Barron, *Encycl. Surf. Colloid Sci.* **2002**, *1*, 1438.
[30] O. Monfort, T. Roch, M. Gregor, L. Satrapinskyy, D. Raptis, P. Lianos, G. Plesch, *J. Environ. Chem. Eng.* **2017**, *5*, 5143.
[31] L. Ismail, C. Ferronato, L. Fine, F. Jaber, J. M. Chovelon, *Appl. Catal., B* **2017**, *201*, 573.
[32] Y. Wang, C. S. Hong, *Water Res.* **1999**, *33*, 2031.
[33] G. Fang, W. Wu, C. Liu, D. D. Dionysiou, Y. Deng, D. Zhou, *Appl. Catal., B* **2017**, *202*, 1.
[34] L. W. Matzek, K. E. Carter, *Chem. Eng. J.* **2017**, *307*, 650.
[35] H. Zhong, Y. Tian, Q. Yang, M. L. Brusseau, L. Yang, G. Zeng, *Chem. Eng. J.* **2017**, *307*, 399.
[36] N. T. Boncagni, J. M. Otaegui, E. Warner, T. Curran, J. Ren, M. M. F. De Cortalezzi, *Environ. Sci. Technol.* **2009**, *43*, 7699.
[37] V. Buscio, S. Brosillon, J. Mendret, M. Crespi, C. Gutiérrez-bouzán, *Materials* **2015**, *8*, 3633.
[38] D. E. Kritikos, N. P. Xekoukoulotakis, E. Psillakis, D. Mantzavinos, *Water Res.* **2007**, *41*, 2236.
[39] J. Zhao, Y. Sun, F. Wu, M. Shi, X. Liu, *J. Chem.* **2019**, *2019*, 1.
[40] T. Olmez-Hanci, I. Arslan-Alaton, *Chem. Eng. J.* **2013**, *224*, 10.
[41] I. M. Kolthoff, I. K. Miller, *J. Am. Chem. Soc.* **1951**, *73*, 3055.
[42] I. M. Kolthoff, I. K. Miller, *J. Am. Chem. Soc.* **1951**, *73*, 5118.
[43] H. Gao, J. Chen, Y. Zhang, X. Zhou, *Chem. Eng. J.* **2016**, *306*, 522.
[44] R. Matta, S. Tlili, S. Chiron, S. Barbati, *Environ. Chem. Lett.* **2011**, *9*, 347.
[45] G. P. Anipsitakis, D. D. Dionysiou, *Environ. Sci. Technol.* **2004**, *38*, 3705.
[46] G. V. Buxton, C. L. Greenstock, W. P. Helman, A. B. Ross, *J. Phys. Chem. Ref. Data* **1988**, *17*, 513.
[47] M. Sabri, A. Habibi-Yangjeh, H. Chand, V. Krishnan, *Sep. Purif. Technol.* **2020**, *250*, 117268.
[48] M. Krebel, H. Kušić, N. Koprivanac, J. Meixner, A. Loncaric Bozic, *J. Environ. Eng.* **2011**, *137*, 639.
[49] M. Cvetnić, A. Tomić, M. Sigurnjak, M. N. Stankov, Š. Ukić, H. Kušić, T. Bolanča, A. L. Božić, *J. Water Process Eng.* **2020**, *33*, 101053.
[50] V. Brlenic, H. Kusic, D. Juretic, A. L. Bozic, *J. Water Process Eng.* **2016**, *10*, 78.
[51] Y. Zhang, Y. Xiao, Y. Zhong, T. T. Lim, *Chem. Eng. J.* **2019**, *372*, 420.
[52] A. G. Trovó, R. F. P. Nogueira, A. Agüera, A. R. Fernandez-Alba, S. Malato, *Water Res.* **2011**, *45*, 1394.
[53] D. Juretic, H. Kusic, D. D. Dionysiou, A. Loncaric Bozic, *J. Hazard. Mater.* **2013**, *262*, 377.
[54] M. J. Farré, M. I. Franch, J. A. Ayllón, J. Peral, X. Domènech, *Desalination* **2007**, *211*, 22.
[55] M. D. Hernando, A. R. Fernandez-Alba, R. Tauler, D. Barcelo, *Talanta* **2005**, *65*, 358.
[56] R. Matta, H. Younes, R. Hanna, R. A. -K. J. Saab, *J. Environ. Manage.* **2019**, *245*, 375.
[57] L. Wojnarovits, T. Toth, E. Takacs, *Crit. Rev. Environ. Sci. Technol.* **2018**, *48*, 575.
[58] Z. Zuo, Z. Cai, Y. Katsumura, N. Chitose, Y. Muroya, *Radiat. Phys. Chem.* **1999**, *55*, 15.
[59] O. P. Chawla, R. W. Fessenden, *J. Phys. Chem.* **1975**, *79*, 2693.
[60] C. Guillard, E. Puzenat, H. Lachheb, A. Houas, J.-M. Herrmann, *Int. J. Photoenergy* **2005**, *7*, 641208.
[61] M. Kwon, S. Kim, Y. Yoon, Y. Jung, T. M. Hwang, J. Lee, J. W. Kang, *Chem. Eng. J.* **2015**, *269*, 379.
[62] D. M. Leech, M. T. Snyder, R. G. Wetzel, *Sci. Total Environ.* **2009**, *407*, 2087.
[63] M. G. Antoniou, C. Zhao, K. E. O'shea, G. Zhang, D. D. Dionysiou, C. Zhao, C. Han, M. N. Nadagouda, H. Choi, T. Fotiou, T. M. Triantis, A. Hiskia, *Photocatalytic Degradation of Organic Contaminants in Water: Process Optimization and Degradation Pathways*, The Royal Society Of Chemistry, London, UK **2016**.
[64] X. Duan, C. Su, L. Zhou, H. Sun, A. Suvorova, T. Odedairo, Z. Zhu, Z. Shao, S. Wang, *Appl. Catal., B* **2016**, *194*, 7.
[65] H. Ding, J. Hu, *Chem. Eng. J.* **2020**, *397*, 125462.
[66] D. Lin, J. Ji, Z. Long, K. Yang, F. Wu, *Water Res.* **2012**, *46*, 4477.